Low-lying states of even-even $N = 80$ isotones within the nucleon-pair approximation

M. Bao,[1,2] H. Jiang,[3,2] Y. M. Zhao,[2,4,*] and A. Arima[2,5]

[1]*Department of Physics, University of Shanghai for Science and Technology, Shanghai 200093, China*
[2]*Shanghai Key Laboratory of Particle Physics and Cosmology, School of Physics and Astronomy, Shanghai Jiao Tong University, Shanghai 200240, China*
[3]*School of Arts and Sciences, Shanghai Maritime University, Shanghai 201306, China*
[4]*Collaborative Innovation Center of IFSA (CICIFSA), Shanghai Jiao Tong University, Shanghai 200240, China*
[5]*Musashi Gakuen, 1-26-1 Toyotamakami Nerima-ku, Tokyo 176-8533, Japan*

(Received 14 February 2019; revised manuscript received 8 November 2019; published 21 January 2020)

In this paper we study low-lying states of even-even $N = 80$ isotones including ^{130}Sn, ^{132}Te, ^{134}Xe, ^{136}Ba, and ^{138}Ce, within the nucleon-pair approximation of the shell model. We calculate low-lying energy levels of these nuclei with both positive and negative parities. The wave functions of yrast $2_1^+ - 10_1^+$ states and $1_1^- - 11_1^-$ states of these nuclei are analyzed in detail. Our calculations show that most of these states have a very simple structure in nucleon-pair basis: the 2_1^+ states of ^{132}Te, ^{134}Xe, ^{136}Ba, and ^{138}Ce are dominated by one D^+ neutron pair and spin $J = 2$ proton excitation; the 4_1^+ and 6_1^+ states of ^{132}Te and ^{134}Xe are dominated by the proton excitation, while the 8_1^+ and 10_1^+ states are dominated by S^+ pairs of protons and one spin-eight and spin-ten pair of valence neutron holes (i.e., seniority-two excitations); for negative-parity states, the lowest states with spin four to seven of ^{132}Te, ^{134}Xe, ^{136}Ba, and ^{138}Ce are essentially given by S^+ pairs of protons and one broken pair with spin four to seven consists of $h_{11/2}d_{3/2}$ valence neutron holes. The necessity of $J = 10$ pairing interaction in the phenomenological monopole plus quadrupole shell-model Hamiltonian for $N = 80$ isotones is demonstrated with analytical formulas for simple nucleon-pair configurations, and the pattern of g factors is discussed based on simple arguments. Our calculated $B(E2)$ transition rates and g factors of the low-lying states are well consistent with the experimental data.

DOI: 10.1103/PhysRevC.101.014316

I. INTRODUCTION

Study of low-lying states in atomic nuclei based on the nuclear shell model (SM) [1–4] is one of the important subjects in nuclear structure theory. In recent decades, the structure of even-even nuclei with the mass number $A \approx 130$ has attracted much attention, and many efforts have been made on the study of low-lying states of nuclei in this region [5–22], within the nucleon-pair approximation of the shell model (NPA) [23,24]. These studies focus on the back-bending phenomenon of yrast states at spin around 8–10, the yrast 10^+ isomers, and the γ instability in low-lying states.

The NPA with only S and D pairs (spin equals 0 and 2) for nuclei in the $A \approx 130$ region is able to describe the ground states and the yrast 2^+, 4^+ states. For higher states, such as the yrast 6^+, 8^+, and 10^+ states, calculated energy levels in terms of only SD nucleon pairs deviate from the experimental data, and pairs with higher spin should be considered [12,15–18]. Since the yrast 10^+ isomers have been reported in even-Z isotones with $N = 80$, from $^{130}_{50}$Sn up to $^{148}_{68}$Er [25–32], the neutron $(h_{11/2})^{-2}$ configuration is suggested to represent these isomeric states. In Ref. [9], most low-lying negative parity states of a few even-even nuclei in this region are interpreted in terms of the NPA by considering SD pairs and collective neutron pairs with negative parity and spin 3 and 8.

This paper aims at studying the low-lying states of a few even-even nuclei with neutron number $N = 80$, i.e., ^{130}Sn, ^{132}Te, ^{134}Xe, ^{136}Ba, and ^{138}Ce within the NPA. We consider the 50–82 major shell with five single-particle orbits including $0g_{7/2}$, $1d_{5/2}$, $1d_{3/2}$, $2s_{1/2}$, and $0h_{11/2}$. Besides S and D pairs, we consider all the above nucleon pairs, i.e., pairs with higher spin, neutron $(h_{11/2})^{-2}$ configuration, and a number of nucleon pairs with negative parity as building blocks of the configuration space, in order to study the low-lying states with both positive parity and negative parity for nuclei in this region. In this paper we show that wave functions of most yrast states for these nuclei are very simple in terms of nucleon-pair basis states. The regular patterns of $B(E2)$ values and g factors are studied in terms of nucleon-pair basis states.

This paper is organized as follows. In Sec. II, we briefly introduce the formulation of the NPA [23,24,33], including the nucleon-pair basis states, the phenomenological SM Hamiltonian, and operators in this approach. The calculated results and discussions are given in Sec. III, and Sec. IV is the summary. In Appendix A we present analytical results of quadrupole operator, which are used in our discussions. In Appendix B we present analytical matrix elements of two-body interaction operators for one or two nucleon-pair basis states.

*Corresponding author: ymzhao@sjtu.edu.cn

TABLE I. Single-particle energies (in MeV) of valence protons and single-hole energies (in MeV) of valence neutron holes, based on yrast state energies of ^{133}Sb and ^{131}Sn [44–46], respectively.

j^{parity}	$1/2^+$	$3/2^+$	$5/2^+$	$7/2^+$	$11/2^-$
$\epsilon_{j\pi}$	2.990	2.690	0.963	0.000	2.760
$\epsilon_{j\nu}$	0.332	0.000	1.655	2.434	0.242

II. FRAMEWORK OF THE NPA

In this section, we give a brief introduction to the nucleon-pair approximation of the shell model (NPA). This method was developed by Chen [23], and was generalized to systems with both even and odd number of nucleons [24], isospin symmetry [34], and particle-hole configurations [35]. We note that in recent years calculations of nucleon-pair truncated shell model with isospin symmetry were performed by Qi *et al.* [36,37] and Isacker *et al.* [38,39], and that generalized seniority approach was studied by Jia [40,41] and Caprio [42,43]. For a recent review, see Ref. [33].

A. Hamiltonian

The Hamiltonian in this paper is defined as

$$H = H_0 + H_P + H_Q. \tag{1}$$

The first term on the right-hand side of Eq. (1) corresponds to the spherical single-particle (-hole) energy, i.e.,

$$H_0 = \sum_{\alpha\sigma} \epsilon_{\alpha\sigma} C^\dagger_{\alpha\sigma} C_{\alpha\sigma}. \tag{2}$$

Here, $C^\dagger_{\alpha\sigma}$ is a creation operator and $C_{\alpha\sigma}$ is an annihilation operator. $\alpha = (nl\,jm)$ denotes all required quantum numbers of a nucleus, and $\sigma = \pi$ or ν corresponds to the degree of freedom of protons or neutrons. In this paper, the single-particle energies of valence protons, $\epsilon_{j\pi}$, are taken from energies of the lowest state with spin j in ^{133}Sb, which has one valence proton outside the core nucleus, ^{132}Sn. Single-hole energies of valence neutron holes, $\epsilon_{j\nu}$, are taken from energies of the lowest state with spin j in ^{131}Sn, which has one valence neutron hole relative to ^{132}Sn. These single-particle (-hole) energies, taken from Refs. [44–46], are tabulated in Table I of this paper.

The second term in Eq. (1), H_P, corresponds to residual interactions between the like valence particles, and in this paper we take

$$H_P = V_0 + V_2 + V_4 + V_{10}. \tag{3}$$

The definitions of V_0, V_2, V_4, and V_{10} are as follows.

$$V_0 = G^{(0)}_\pi \mathcal{P}^{(0)\dagger}_\pi \cdot \tilde{\mathcal{P}}^{(0)}_\pi + G^{(0)}_\nu \mathcal{P}^{(0)\dagger}_\nu \cdot \tilde{\mathcal{P}}^{(0)}_\nu \tag{4}$$

is the monopole pairing interaction, with

$$\mathcal{P}^{(0)\dagger}_\sigma = \sum_{a_\sigma} \frac{\hat{j}_\sigma}{2} (C^\dagger_{a_\sigma} \times C^\dagger_{a_\sigma})^{(0)}_0,$$

$$\tilde{\mathcal{P}}^{(0)}_\sigma = -\sum_{a_\sigma} \frac{\hat{j}_\sigma}{2} (\tilde{C}_{a_\sigma} \times \tilde{C}_{a_\sigma})^{(0)}_0,$$

where $\hat{j}_\sigma = \sqrt{2j_\sigma + 1}$;

$$V_2 = G^{(2)}_\pi \mathcal{P}^{(2)\dagger}_\pi \cdot \tilde{\mathcal{P}}^{(2)}_\pi + G^{(2)}_\nu \mathcal{P}^{(2)\dagger}_\nu \cdot \tilde{\mathcal{P}}^{(2)}_\nu \tag{5}$$

is the quadrupole pairing interaction, with

$$\mathcal{P}^{(t)\dagger}_{\sigma M} = \sum_{a_\sigma b_\sigma} q(a_\sigma b_\sigma t)(C^\dagger_{a_\sigma} \times C^\dagger_{b_\sigma})^{(t)}_M,$$

$$\tilde{\mathcal{P}}^{(t)}_{\sigma M} = -\sum_{a_\sigma b_\sigma} q(a_\sigma b_\sigma t)(\tilde{C}_{a_\sigma} \times \tilde{C}_{b_\sigma})^{(t)}_M, \tag{6}$$

where $t = 2$, $M = 0, \pm 1$, or ± 2,

$$q(ab\lambda) = -\frac{1}{\hat{\lambda}} \frac{\langle j_a || r^\lambda Y^\lambda || j_b \rangle}{r^\lambda_0}, \tag{7}$$

with r_0 being the oscillator parameter ($r_0^2 = 1.012A^{1/3}$ fm^2), and the expression of $q(ab\lambda)$ for a single-j shell is summarized in Appendix A;

$$V_4 = G^{(4)}_\nu \mathcal{P}^{(4)\dagger}_\nu \cdot \tilde{\mathcal{P}}^{(4)}_\nu, \tag{8}$$

where $\mathcal{P}^{(4)\dagger}_\nu$ and $\tilde{\mathcal{P}}^{(4)}_\nu$ are defined in Eq. (6) with $t = 4$; and

$$V_{10} = G^{(10)}_\nu \mathcal{P}^{(10)\dagger}_\nu \cdot \tilde{\mathcal{P}}^{(10)}_\nu, \tag{9}$$

where

$$\mathcal{P}^{(10)\dagger}_\nu = (C^\dagger_j \times C^\dagger_j)^{(10)}_M, \quad \tilde{\mathcal{P}}^{(10)}_\nu = -\left(\tilde{C}_j \times \tilde{C}_j\right)^{(10)}_M,$$

with j corresponding to the neutron $h_{11/2}$ orbit.

The last term in Eq. (1) is

$$H_Q = V_Q + V_{Q_{\pi\nu}}. \tag{10}$$

Here

$$V_Q = \sum_\sigma \kappa^{(2)}_\sigma Q^{(2)}_\sigma \cdot Q^{(2)}_\sigma \tag{11}$$

corresponds to the quadrupole-quadrupole interaction between the like valence nucleons, with the operator

$$Q^{(2)}_{\sigma M} = \sum_{ab} q(ab2)(C^\dagger_{a_\sigma} \times \tilde{C}_{b_\sigma})^{(2)}_M, \tag{12}$$

where $q(ab2)$ is given by Eq. (7). $V_{Q_{\pi\nu}}$ in Eq. (10) corresponds to the proton-neutron interaction, which is defined as

$$V_{Q_{\pi\nu}} = \kappa Q^{(2)}_\pi \cdot Q^{(2)}_\nu. \tag{13}$$

The interaction parameters for ^{130}Sn, ^{132}Te, ^{134}Xe, ^{136}Ba, and ^{138}Ce are tabulated in Table II.

B. Configuration basis

We define a noncollective nucleon pair with spin r and projection μ,

$$A^r_\mu(ab)^\dagger = (C^\dagger_a \times C^\dagger_b)^{(r)}_\mu, \tag{14}$$

where a and b are angular momenta of a single-particle orbit. The time reversal of $A^r_\mu(ab)^\dagger$ is

$$\tilde{A}^r_\mu(ab) = -(\tilde{C}_a \times \tilde{C}_b)^{(r)}_\mu, \tag{15}$$

with the convention $\tilde{C}_{jm} = (-1)^{j-m} C_{j-m}$.

TABLE II. Interaction parameters of ^{130}Sn, ^{132}Te, ^{134}Xe, ^{136}Ba, and ^{138}Ce. $G_\nu^{(0)}$, $G_\pi^{(0)}$, and $G_\nu^{(10)}$ are in units of MeV, $G_\nu^{(4)}$ is in units of MeV/r_0^8, and other parameters are in units of MeV/r_0^4. We adopt constant interaction parameters of $G_\nu^{(0)}$, $G_\pi^{(0)}$, $G_\pi^{(2)}$, and $G_\nu^{(4)}$, and assume smooth change of $G_\nu^{(2)}$, $G_\nu^{(10)}$, $\kappa_\nu^{(2)}$, $\kappa_\pi^{(2)}$, and κ with valence proton number N_π.

$G_\nu^{(0)}$	$G_\nu^{(2)}$	$G_\nu^{(4)}$	$G_\nu^{(10)}$	$\kappa_\nu^{(2)}$
-0.168	$-0.019 - 0.0005N_\pi$	-0.0002	$0.050 + 0.035N_\pi$	$-0.013 - 0.0035N_\pi$
$G_\pi^{(0)}$	$G_\pi^{(2)}$	$\kappa_\pi^{(2)}$	κ	
-0.180	-0.027	$-0.065 + 0.0035N_\pi$	$0.050 + 0.005N_\pi$	

A collective nucleon pair is defined as

$$A_\mu^{r\dagger} = \sum_{ab} y(abr)(C_a^\dagger \times C_b^\dagger)_\mu^{(r)}, \tag{16}$$

where $y(abr)$ is the structure coefficient of the collective pair A^r, with the symmetry

$$y(abr) = (-1)^{a+b+r+1} y(bar). \tag{17}$$

There are many approaches to obtain $y(abr)$, as introduced in Ref. [33]. In this paper, the procedure to obtain $y(abr)$ is same as given in Ref. [47]. The time reversal of $A_\mu^{r\dagger}$ is

$$\tilde{A}_\mu^r = -\sum_{ab} y(abr)(\tilde{C}_a \times \tilde{C}_b)_\mu^{(r)}. \tag{18}$$

For a $2n$ identical-nucleon system, we couple n nucleon pairs successively to construct a nucleon-pair basis state,

$$\begin{aligned} |\tau J_n M_n\rangle &\equiv A_{M_n}^{J_n\dagger}(r_i, J_i)|0\rangle \\ &\equiv A_{M_n}^{J_n\dagger}(r_1 r_2 \cdots r_n, J_1 J_2 \cdots J_n)|0\rangle \\ &= [\cdots (A^{r_1\dagger} \times A^{r_2\dagger})^{(J_2)} \times \cdots \times A^{r_n\dagger}]_{M_n}^{(J_n)}|0\rangle. \end{aligned} \tag{19}$$

Here τ is the abbreviation, which represents all the necessary intermediate quantum numbers. $J_1 = r_1$, J_n is the total angular momentum of these $2n$ nucleons, and M_n is the z component of J_n. The time reversal of the operator $A_{M_n}^{J_n\dagger}(r_i, J_i)$ is

$$\begin{aligned} \tilde{A}_{M_n}^{J_n}(r_i, J_i) &\equiv \tilde{A}_{M_n}^{J_n}(r_1 r_2 \cdots r_n, J_1 J_2 \cdots J_n) \\ &= [\cdots (\tilde{A}^{r_1} \times \tilde{A}^{r_2})^{(J_2)} \times \cdots \times \tilde{A}^{r_n}]_{M_n}^{(J_n)}. \end{aligned} \tag{20}$$

In this paper S, D, F, G, H, I, and $\mathcal{J}$ represent a nucleon pair with spin 0, 2, 3, 4, 5, 6, and 7, respectively (the symbol J, which is used to label state spin is avoided here). For proton degree of freedom, collective S^+, D^+, G^+, I^+, and I'^+ (the second spin-six) pairs are taken to construct the proton nucleon-pair basis states, except for ^{138}Ce for which collective S^+, D^+ proton pairs and up to one G^+ proton pair, one I^+ proton pair and one I'^+ proton pair are considered due to computational cost. Because the spin alignment of neutron $(h_{11/2})^{-2}$ contributes to the yrast 10^+ state and gives rise to back bending [48,49], we construct the neutron configuration space of ^{130}Sn, ^{132}Te, ^{134}Xe, ^{136}Ba, and ^{138}Ce by collective S^+, S'^+ (the second spin-zero) and D^+ pairs together with the noncollective $(h_{11/2})_{10}^{-2}$ pairs (denoted by $\mathcal{A}^{(J)}$ with spin $J = 2, 4, 6, 8, 10$). To calculate the energy levels with negative parity, we also take collective F^-, G^-, H^-, I^-, and $\mathcal{J}^-$ pairs for neutrons into consideration; the proton pairs with negative parity are not important in low-lying states of these nuclei because the single-particle energy of the proton $h_{11/2}$ orbit is large (2.760 MeV, see Table I). In this paper, the basis states based on these pairs are normalized but nonorthogonal to each other.

C. Electromagnetic-transition operators

The electromagnetic-transition operators in this paper are defined as

$$T(E2) = \sum_\sigma e_\sigma r_\sigma^2 Y_\sigma^2, \tag{21}$$

$$T(M1) = \sqrt{\frac{3}{4\pi}} \sum_\sigma (g_{l\sigma}\vec{L}_\sigma + g_{s\sigma}\vec{S}_\sigma). \tag{22}$$

Here $e_\sigma = e_\pi$, e_ν (in units of e) correspond to effective charges (including bare charges) of valence protons and valence neutron holes, respectively. $g_{l\sigma}$ and $g_{s\sigma}$ (in unit of $\mu_N/\hbar$) are orbital and spin gyromagnetic ratios of valence nucleons, respectively. In this paper, we take $e_\pi = 1.79$, $e_\nu = -0.71$, $g_{l\pi} = 1.00$, $g_{l\nu} = 0.02$, $g_{s\pi} = 5.586 \times 0.7$, and $g_{s\nu} = -3.826 \times 0.7$. Namely, we take the quenching factor for the spin part of magnetic moment to be its conventional value, 0.7. L_σ and S_σ in Eq. (22) are the total orbital angular momentum operator and the total spin operator, and are defined as below, respectively.

$$\begin{aligned} L_\sigma &= Q_{l\sigma}^{(1)} = \sum_{ab} q_l(ab1)(C_a^\dagger \times \tilde{C}_b)^{(1)}, \\ S_\sigma &= Q_{s\sigma}^{(1)} = \sum_{ab} q_s(ab1)(C_a^\dagger \times \tilde{C}_b)^{(1)}, \end{aligned}$$

where

$$\begin{aligned} q_l(ab1) &= (-1)^{l+b+1/2}\sqrt{\frac{l(l+1)}{3}}\hat{a}\hat{b}\hat{l}\begin{Bmatrix} a & b & 1 \\ l & l & 1/2 \end{Bmatrix}, \\ q_s(ab1) &= (-1)^{l+a+1/2}\sqrt{\frac{1}{2}}\hat{a}\hat{b}\begin{Bmatrix} a & b & 1 \\ l/2 & l/2 & l \end{Bmatrix}. \end{aligned}$$

Here "{ }" denotes the six-j symbol. The magnetic moment of state Ψ_{JM} is defined by

$$\begin{aligned} \mu &= \langle \Psi_{JM}|\hat{\mu}_z|\Psi_{JM}\rangle_{M=J}, \\ \hat{\mu} &= \sqrt{\frac{4\pi}{3}}T(M1), \end{aligned} \tag{23}$$

and the g factor equals μ/J, where J is the total angular momentum.

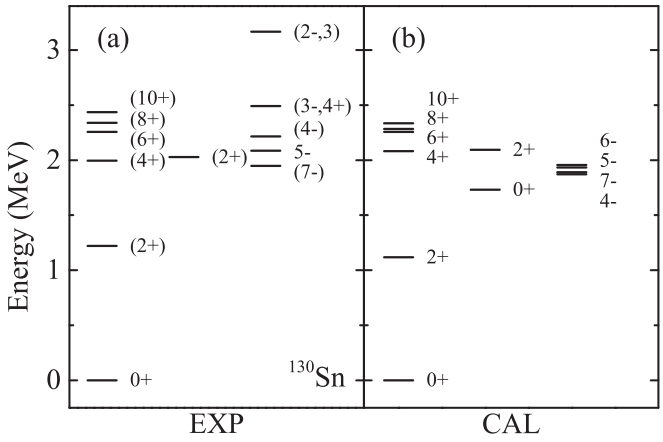

FIG. 1. Energy levels of ^{130}Sn. (a) is the experimental data [46], and (b) is our calculated results by using the coefficients given in Table II.

III. RESULTS AND DISCUSSIONS

In this section, we present our calculated results of ^{130}Sn, ^{132}Te, ^{134}Xe, ^{136}Ba, and ^{138}Ce. Our calculated energy levels for these five nuclei are plotted in Fig. 1 and Fig. 2, and are compared with the experimental database of Ref. [46]. It is shown that the energy levels of most low-lying states are well reproduced. For each nucleus, we present our calculated $B(E2)$ transition rates (in units of W.u.) and g factors (in unit of μ_N) for low-lying states, respectively, in Table III and Table IV, and compare them with experimental data [26,32,46,50–52]. One sees that our calculated $B(E2)$ and g-factor results reasonably agree with experimental data.

Below we first discuss low-lying states of ^{130}Sn, then go on to discuss the 2_1^+–10_1^+ states and negative parity 1_1^-–11_1^- states for ^{132}Te, ^{134}Xe, ^{136}Ba, and ^{138}Ce, and finally discuss the robustness of parameters of the Hamiltonian.

A. ^{130}Sn nucleus

The ^{130}Sn nucleus has only two valence neutron holes, matrix elements of the Hamiltonian can be calculated analytically; as shown in the Appendix B, the V_0, V_2, and V_4 terms of the Hamiltonian contribute to states with spin 0, 2, and 4, respectively, but not to states with other spins. For two valence neutron holes in the 50–82 major shell, the 8_1^+ and 10_1^+ states are given by two valence neutron holes in the $h_{11/2}$ orbit. According to Eq. (A3) and Eq. (B24), one sees that the matrix element of $Q^{(2)} \cdot Q^{(2)}$ equals $\frac{6125}{484\pi} \approx 4.028$ and $\frac{1075}{44\pi} \approx 7.777$ for $J = 8$ and 10, respectively. Assuming a negative value of $\kappa_\nu^{(2)}$ and the Hamiltonian defined in Eqs. (1), (3), and (10), obviously the energy of the 8_1^+ state would be lower than that of the 10_1^+ state on condition that one adopts a positive value of $G_\nu^{(10)}$ in the $\mathcal{P}_\nu^{(10)\dagger} \cdot \tilde{\mathcal{P}}_\nu^{(10)}$ term.

B. 2^+ states

We first look at the configurations for the two lowest 2^+ states of ^{132}Te. In Ref. [53], the dominant components of the 2_1^+ state were suggested to be $0.74|\nu^{-2}, 2^+\rangle \otimes |\pi^2, 0^+\rangle + 0.67|\nu^{-2}, 0^+\rangle \otimes |\pi^2, 2^+\rangle$; in Ref. [54], the dominant components of the wave function for the 2_1^+ state are $0.62|\nu^{-2}, 2^+\rangle \otimes |\pi^2, 0^+\rangle + 0.66|\nu^{-2}, 0^+\rangle \otimes |\pi^2, 2^+\rangle$, and that of the 2_2^+ state are $-0.63|\nu^{-2}, 2^+\rangle \otimes |\pi^2, 0^+\rangle + 0.58|\nu^{-2}, 0^+\rangle \otimes |\pi^2, 2^+\rangle$. In our calculation, the wave functions of the 2_1^+ and 2_2^+ states are

$$\begin{aligned} \left|2_1^+\right\rangle &= 0.66\left|D_\nu^+ \otimes S_\pi^+\right\rangle + 0.74\left|S_\nu^+ \otimes D_\pi^+\right\rangle + \cdots, \\ \left|2_2^+\right\rangle &= -0.74\left|D_\nu^+ \otimes S_\pi^+\right\rangle + 0.66\left|S_\nu^+ \otimes D_\pi^+\right\rangle + \cdots, \end{aligned} \tag{24}$$

respectively, which are in reasonable agreement with theoretical results of Refs. [53,54].

According to the proton-neutron interacting boson model [55], low-lying states of atomic nuclei are characterized by

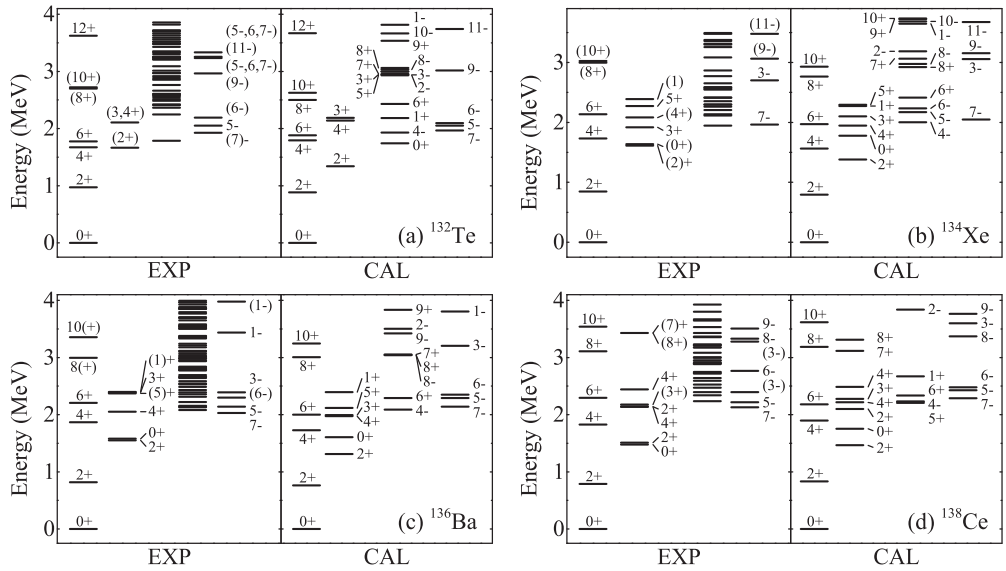

FIG. 2. Energy levels of ^{132}Te, ^{134}Xe, ^{136}Ba, and ^{138}Ce, presented in (a), (b), (c), and (d), respectively. The left-hand side in each panel corresponds to experimental data [46], and the right-hand side corresponds to our NPA calculated results.

TABLE III. $B(E2)$ values (in units of W.u.) of ^{130}Sn, ^{132}Te, ^{134}Xe, ^{136}Ba, and ^{138}Ce. Experimental data are taken from Refs. [26,32,46,50,51].

	^{130}Sn		^{132}Te		^{134}Xe		^{136}Ba		^{138}Ce	
$J_i \to J_f$	Expt.	Cal.	Expt.	Cal.	Expt.	Cal.	Expt.	Cal.	Expt.	Cal.
$2_1^+ \to 0_1^+$	1.18	1.45	10(1)	9.02	15.3(11)	15.28	19^{+2}_{-1}	19.75	21.2(14)	21.27
$2_2^+ \to 0_1^+$	–	0.003	0.5(1)	0.49	0.74(5)	0.49	0.78(19)	0.04	1.16(8)	1.07
$2_2^+ \to 2_1^+$	–	1.60	–	0.38	20(2)	8.08	15(4)	17.96	28(2)	25.36
$4_1^+ \to 2_1^+$	–	0.45	–	8.32	11.6(8)	12.67	14(6)	24.14	–	28.19
$6_1^+ \to 4_1^+$	–	1.13	3.3(2)	3.41	–	7.94	0.574(25)	0.28	0.113(9)	0.078
$8_1^+ \to 6_1^+$	–	0.70	–	<0.001	–	0.015	–	6.72	–	8.55
$10_1^+ \to 8_1^+$	0.38(4)	0.26	1.05(3)	0.96	160(50)/0.64(1)	1.68	0.023(2)	<0.001	0.011(3)	<0.001
$5_1^- \to 7_1^-$	1.4(2)/1.16(7)	0.61	–	2.54	–	4.46	6.0(11)	5.35	290(8)	7.84

F spin. The states with maximum ***F*** spin are called the fully symmetric states (FSSs), while the others with nonmaximum ***F*** spin are called the mixed-symmetric states (MSSs). The experimental data given in Ref. [54] suggest that the 2_2^+ state of ^{132}Te decays to the ground state with a weak $E2$ transition and to the 2_1^+ state (FSS) with a strong $M1$ transition, and in Ref. [16] the 2_2^+ state of ^{132}Te at 1.665 MeV is predicted to be the lowest MSS. The wave functions in Eq. (24) and calculated $B(E2)$ values in Table III exhibit a consistent pattern.

We calculate the overlap squared between the neutron (or proton) excitation configuration and the wave function of the 2_1^+ states, and plot them versus the mass number A in Fig. 3. Black squares correspond to the $|D_\nu^+\rangle \otimes |(S_\pi^+)^{N_\pi/2}, J_\pi = 0\rangle$ configuration (namely neutron excitation), and red circles correspond to the $|S_\nu^+\rangle \otimes |J_\pi = 2\rangle$ configuration (namely proton excitation). Here the neutron excitation configuration means that all protons are S pairs, and proton excitation configuration means that the valence neutron hole pair in the 50–82 shell is an S pair while the total spin of valence protons, J_π, equals two. One sees from Fig. 3 that these two excitation modes are two dominant components in the wave function of the 2_1^+ state of ^{132}Te, ^{134}Xe, ^{136}Ba, and ^{138}Ce, while the other configurations are negligible.

In Fig. 4, we plot the $B(E2; 2_1^+ \to 0_1^+)$ values and g factors of the 2_1^+ states versus the mass number A. The experimental data [32,46,50] and results of Refs. [17,18,56–58] are also plotted for comparison. It is shown in Fig. 4(a) that the $B(E2; 2_1^+ \to 0_1^+)$ values increase with the mass number A, and our calculated results agree with the experimental data very well. However, for the $g_{2_1^+}$ value of ^{138}Ce given in Fig. 4(b), neither our presented result nor the previous PTSM calculation [17] well fit the experimental data, and this deviation should be further investigated in the future.

C. 4_1^+ and 6_1^+ states

The ^{132}Te nucleus has two valence neutron holes and two valence protons with respect to the ^{132}Sn nucleus, thus one easily conjectures that the 4_1^+ and 6_1^+ states of ^{132}Te might be understood based on the low-lying levels of ^{130}Sn and ^{134}Te. As the 4_1^+ and 6_1^+ states of ^{134}Te (1.576 and 1.691 MeV) lie much lower than those of ^{130}Sn (1.996 and 2.257 MeV), the 4_1^+ and 6_1^+ states of the ^{132}Te nucleus are usually assumed to be seniority-two states of proton excitation dominantly [59–61]; e.g., Ref. [59] suggested that $|4_1^+\rangle = 0.97|0_1^+(\nu)\rangle \otimes |4_1^+(\pi)\rangle$ and $|6_1^+\rangle = 0.97|0_1^+(\nu)\rangle \otimes |6_1^+(\pi)\rangle$, and Ref. [61] suggested that the proton excitation configuration occupies about 78% or 85% in the wave function of the 4_1^+ state, and about 82% or 87% of the 6_1^+ state. The configuration from D pair of two valence neutron holes is small in the wave functions of the 4_1^+ and 6_1^+ states.

In our NPA calculation, the wave functions of the 4_1^+ and 6_1^+ states of ^{132}Te in terms of nucleon pairs are

$$|4_1^+\rangle = 0.86|S_\nu^+ \otimes G_\pi^+\rangle + \cdots,$$
$$|6_1^+\rangle = 0.97|S_\nu^+ \otimes J_\pi = 6\rangle + \cdots, \quad (25)$$

TABLE IV. g factors (in units of μ_N) of ^{130}Sn, ^{132}Te, ^{134}Xe, ^{136}Ba, and ^{138}Ce. Experimental data are taken from Ref. [46] except for ^{130}Sn taken from Ref. [52].

	^{130}Sn		^{132}Te		^{134}Xe		^{136}Ba		^{138}Ce	
J	Expt.	Cal.	Expt.	Cal.	Expt.	Cal.	Expt.	Cal.	Expt.	Cal.
2_1^+	–	0.006	0.28(15)/(+)0.46(5)	0.424	0.354(7)/0.56(10)	0.484	0.34(5)	0.532	0.26(8)	0.494
4_1^+	–	−0.225	–	0.593	0.80(15)	0.638	–	0.619	–	0.718
6_1^+	–	−0.225	0.79(9)	0.682	–	0.662	–	0.679	–	0.888
8_1^+	–	−0.225	–	−0.221	–	−0.210	–	0.636	–	0.688
10_1^+	–	−0.225	–	−0.221	–	−0.216	–	−0.212	−0.176(10)	−0.186
7_1^-	−0.054	−0.053	–	−0.047	–	−0.037	–	−0.028	–	−0.015

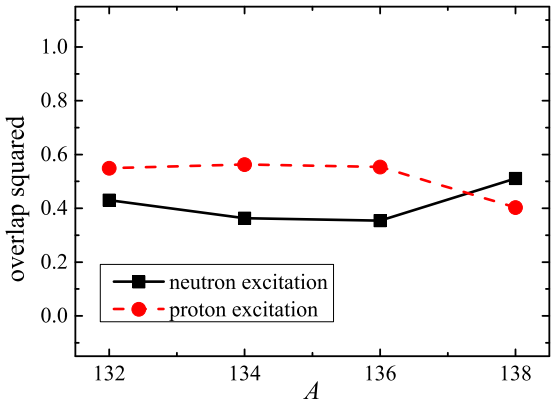

FIG. 3. The overlap squared between the neutron (or proton) excitation configuration and the NPA wave function of the 2_1^+ states, versus the mass number A. The black squares and the red circles correspond to neutron excitation and proton excitation components, respectively.

respectively. Clearly, the dominant components of our calculated 4_1^+ and 6_1^+ states are the proton excitation, with small mixings of D^+ pair consisted of two neutron holes. This result is consistent with the picture of Ref. [61], except that our results suggest that the configuration of proton excitation is

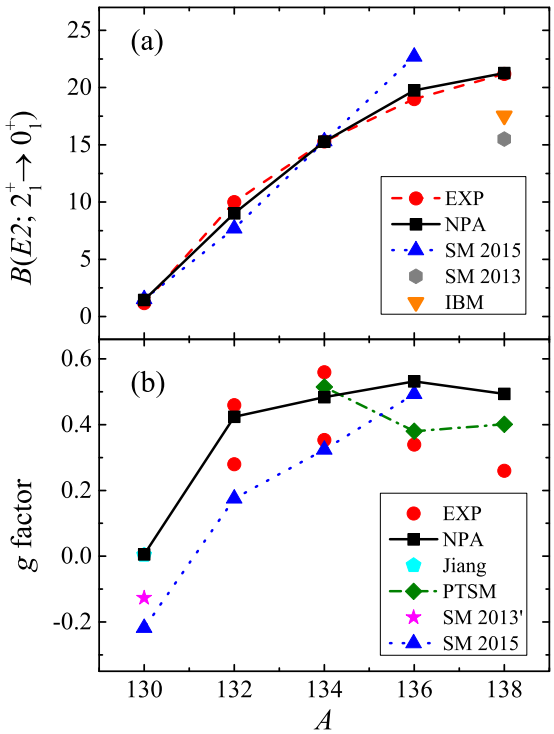

FIG. 4. $B(E2; 2_1^+ \rightarrow 0_1^+)$ and g factors of the 2_1^+ states versus the mass number A. The black squares, blue up triangles, gray hexagon, orange down triangle, green diamonds, pink star, and cyan pentagon correspond to our calculated results by using the NPA, results by the SM 2015 [18], the SM 2013 [56], the IBM [57], the PTSM [17], the SM 2013′ [58], and Jiang [11], respectively. Solid circles in red are the experimental data taken from Refs. [32,46,50].

even more dominant for the 6_1^+ state. This is also the reason why one must include the collective proton G^+ and I^+ pairs as building blocks of the nucleon-pair basis states.

The proton excitation picture of the ^{132}Te nucleus can be understood from a simple perspective of single-j shells (protons in the $g_{7/2}$ orbit and neutron holes in the $h_{11/2}$ orbit). This single-j assumption is supported by their single-particle energies (see I): for protons the lowest single-particle orbit is the $g_{7/2}$, and the next single-particle orbit $d_{5/2}$ is higher than the $g_{7/2}$ by 0.963 MeV; for valence neutron holes, there are three single-particle orbits, $s_{1/2}$, $d_{3/2}$, and $h_{11/2}$, whose energy is very low, and by using two neutron holes in these three orbits (i.e., neglecting the two higher orbits, $d_{5/2}$ and $g_{7/2}$), the only possible way to construct nucleon-pair with spin 4 and 6 is the configuration of $(h_{11/2})^2$. As shown in Sec. II B, we denote these pairs by G_π^+, I_π^+, $\mathcal{A}_\nu^{(4)}$, and $\mathcal{A}_\nu^{(6)}$, respectively.

To proceed our discussion, for both valence protons and valence neutrons, we consider the S^+ and G^+ ($\mathcal{A}^{(4)}$) pairs in the 4_1^+ state, the S^+ and I^+ ($\mathcal{A}^{(6)}$) pairs in the 6_1^+ state. By using Eqs. (B13) and (B24) in Appendix B, or alternatively by using the coefficients of fractional parentage for a $j = 7/2$ orbit in Ref. [62], we analytically obtain energies of the Hamiltonian H_P and H_Q in single-j shells (and H_0 in many-j shells), and present them in Table V. Here for H_P and H_Q, we accordingly assume that the valence protons occupy the $g_{7/2}$ orbit and the valence neutron holes occupy the $h_{11/2}$ orbit. According to Table V, for the 4^+ state,

$$\begin{aligned} \langle S_\nu^+ \otimes G_\pi^+ | H | S_\nu^+ \otimes G_\pi^+ \rangle &\approx -0.883 \text{ MeV}, \\ \left\langle \mathcal{A}_\nu^{(4)} \otimes S_\pi^+ \middle| H \middle| \mathcal{A}_\nu^{(4)} \otimes S_\pi^+ \right\rangle &\approx -0.488 \text{ MeV}, \end{aligned} \tag{26}$$

where we have suppressed the quantum numbers J_π, J_ν, and J in nucleon-pair basis states without confusion. One sees that the energy of $|\mathcal{A}_\nu^{(4)} \otimes S_\pi^+\rangle$ is higher than that of $|S_\nu^+ \otimes G_\pi^+\rangle$ by 0.395 MeV. Then it is understandable that the lowest 4^+ state is dominated by $|S_\nu^+ \otimes G_\pi^+\rangle$ configuration, i.e., the proton excitation. Similarly, from Table V, for the 6^+ state,

$$\begin{aligned} \left\langle S_\nu^+ \otimes I_\pi^+ | H | S_\nu^+ \otimes I_\pi^+ \right\rangle &\approx -0.908 \text{ MeV}, \\ \left\langle \mathcal{A}_\nu^{(6)} \otimes S_\pi^+ \middle| H \middle| \mathcal{A}_\nu^{(6)} \otimes S_\pi^+ \right\rangle &\approx -0.283 \text{ MeV}, \end{aligned} \tag{27}$$

namely, the energy of $|\mathcal{A}_\nu^{(6)} \otimes S_\pi^+\rangle$ is higher than that of $|S_\nu^+ \otimes I_\pi^+\rangle$ by 0.625 MeV. Thus 6_1^+ state is also expected to be dominated by the proton excitation.

For the ^{134}Xe nucleus, our calculated wave functions of the 4_1^+ and 6_1^+ states are,

$$\begin{aligned} |4_1^+\rangle &= 0.87 |S_\nu^+ \otimes J_\pi = 4\rangle + \cdots, \\ |6_1^+\rangle &= 0.94 |S_\nu^+ \otimes J_\pi = 6\rangle + \cdots, \end{aligned} \tag{28}$$

respectively (here the quantum numbers J_ν and J are suppressed). Again, our calculated wave functions of these two states are also dominated by the proton excitation. Below we present an explanation of this picture in terms of single-j shells, as above for the 4_1^+ and 6_1^+ states of ^{132}Te. By using Eqs. (B15) and (B25) in Appendix B, we obtain analytically energies of the Hamiltonian in the nucleon-pair basis states

TABLE V. Matrix elements (in MeV) of H_0, V_0, V_2, and V_Q, for a few simple nucleon-pair basis states with the phenomenological SM Hamiltonian. Results on the left part correspond to ^{132}Te, and those on the right part correspond to ^{134}Xe. The matrix elements of single-particle energies H_0 are calculated in many-j shells. The results of V_0, V_2, V_4, and V_Q are for single-j shells, valence protons in the $g_{7/2}$ orbit and two valence neutron holes in the $h_{11/2}$ orbit; these matrix elements are derived analytically by using Eqs. (B13), (B15) and Eqs. (B23), (B25) in Appendix B. Both V_{10} and $V_{Q_{\pi\nu}}$ equal zero in these nucleon-pair basis states with such single-j shells, and are not included here. Here we exemplify the user manual of this Table by the matrix element $\langle S^+_\nu \otimes G^+_\pi | H | S^+_\nu \otimes G^+_\pi \rangle$ as follows. $\langle S^+_\nu \otimes G^+_\pi | H | S^+_\nu \otimes G^+_\pi \rangle = \langle S^+_\nu | H_0 + V_0 + V_Q | S^+_\nu \rangle + \langle G^+_\pi | H_0 + V_Q | G^+_\pi \rangle = 0.637 - \frac{126}{125} - \frac{91}{88\pi} + 0.039 - \frac{3509}{5040\pi} \approx -0.883$ MeV.

^{132}Te	H_0	$-V_0$	$-V_2$	$-V_4$	$-V_Q$	^{134}Xe	H_0	$-V_0$	$-V_2$	$-V_4$	$-V_Q$
		$\frac{126}{125}$			$\frac{91}{88\pi}$			$\frac{126}{125}$			$\frac{2457}{1760\pi}$
S^+_ν	0.637		0	0		S^+_ν	0.638		0	0	
				$\frac{819}{2200\pi}$	$\frac{635}{968\pi}$					$\frac{819}{2200\pi}$	$\frac{3429}{3872\pi}$
$\mathcal{A}^{(4)}_\nu$	0.484	0	0			$\mathcal{A}^{(4)}_\nu$	0.484	0	0		
					$\frac{371}{968\pi}$						$\frac{10017}{19360\pi}$
$\mathcal{A}^{(6)}_\nu$	0.484	0	0	0		$\mathcal{A}^{(6)}_\nu$	0.484	0	0	0	
		$\frac{18}{25}$			$\frac{3509}{1680\pi}$			$\frac{27}{25}$	$\frac{363}{560\pi}$		$\frac{2057}{840\pi}$
S^+_π	0.740		0	0		$S^+_\pi S^+_\pi$	1.647			0	
					$\frac{3509}{5040\pi}$			$\frac{9}{25}$	$\frac{363}{560\pi}$		$\frac{2057}{1680\pi}$
G^+_π	0.039	0	0	0		$S^+_\pi G^+_\pi$	1.179			0	
					$\frac{3509}{5040\pi}$			$\frac{9}{25}$	$\frac{363}{560\pi}$		$\frac{2057}{1680\pi}$
I^+_π	0.014	0	0	0		$S^+_\pi I^+_\pi$	1.171			0	

with the same single-j shells as for ^{132}Te, and list the results in Table V. Here we consider results for three basis states, i.e., $|S^+_\pi S^+_\pi\rangle$, $|S^+_\pi G^+_\pi\rangle$ and $|S^+_\pi I^+_\pi\rangle$. According to Table V,

$$\begin{aligned}
\langle \mathcal{A}^{(4)}_\nu \otimes S^+_\pi S^+_\pi | H | \mathcal{A}^{(4)}_\nu \otimes S^+_\pi S^+_\pi \rangle &\approx -0.335 \text{ MeV}, \\
\langle S^+_\nu \otimes S^+_\pi G^+_\pi | H | S^+_\nu \otimes S^+_\pi G^+_\pi \rangle &\approx -0.591 \text{ MeV}, \\
\langle \mathcal{A}^{(6)}_\nu \otimes S^+_\pi S^+_\pi | H | \mathcal{A}^{(6)}_\nu \otimes S^+_\pi S^+_\pi \rangle &\approx -0.100 \text{ MeV}, \\
\langle S^+_\nu \otimes S^+_\pi I^+_\pi | H | S^+_\nu \otimes S^+_\pi I^+_\pi \rangle &\approx -0.599 \text{ MeV}.
\end{aligned}$$

We can see that the energy of $|S^+_\nu \otimes S^+_\pi G^+_\pi\rangle$ is much lower than that of $|\mathcal{A}^{(4)}_\nu \otimes S^+_\pi S^+_\pi\rangle$, and the energy of $|S^+_\nu \otimes S^+_\pi I^+_\pi\rangle$ is much lower than that of $|\mathcal{A}^{(6)}_\nu \otimes S^+_\pi S^+_\pi\rangle$. Therefore, one expects that the 4^+_1 and 6^+_1 states of ^{134}Xe are dominated by the proton excitation.

On the other hand, from single-j shell assumption one gets degenerate states for $|S^+_\nu \otimes G^+_\pi\rangle$ and $|S^+_\nu \otimes I^+_\pi\rangle$ of ^{132}Te, and for $|S^+_\nu \otimes S^+_\pi G^+_\pi\rangle$ and $|S^+_\nu \otimes S^+_\pi I^+_\pi\rangle$ of ^{134}Xe, as shown in the matrix elements of V_0, V_2, V_4, and V_Q. This degeneracy is removed by configuration mixings of other single-particle orbits. The mixings from the $d_{5/2}$ orbit play an important role in collective G^+_π and I^+_π pairs, and this can be easily seen from the matrix elements of $\langle G^+_\pi | H_0 | G^+_\pi\rangle$ and $\langle I^+_\pi | H_0 | I^+_\pi\rangle$, which are sizably lower than $\langle \mathcal{A}^{(4)}_\nu | H_0 | \mathcal{A}^{(4)}_\nu\rangle$ and $\langle \mathcal{A}^{(6)}_\nu | H_0 | \mathcal{A}^{(6)}_\nu\rangle$. For ^{134}Xe, the proton excitation configurations of the 4^+_1 state has considerably large mixings of $|S^+_\pi G^+_\pi\rangle$ and $|G^+_\pi G^+_\pi, J_\pi = 4\rangle$. Our numerical results show that this leads to a relatively larger energy splitting between the 4^+_1 and 6^+_1 states. Figures 2(a) and 2(b) well represent both the quasidegeneracy of the 4^+_1 and 6^+_1 states for ^{132}Te, and the relatively larger splitting of the 4^+_1 and 6^+_1 states for ^{134}Xe.

The overlap squared of the proton excitation components, namely, $|S^+_\nu\rangle \otimes |J_\pi = 4\rangle$ for the 4^+_1 states and $|S^+_\nu\rangle \otimes |J_\pi = 6\rangle$ for the 6^+_1 states, with our NPA corresponding wave functions, versus the mass number A, are plotted in Fig. 5. The black squares and the red circles correspond to the 4^+_1 and 6^+_1 states, respectively. One sees that for all these nuclei the 6^+_1 states are dominated by the proton excitation; on the other hand, the 4^+_1 states of these nuclei (in particular for ^{136}Ba and ^{138}Ce) are not well represented by proton excitations, and neutron excitations become more and more important. That is partly the reason why our calculated $B(E2; 6^+_1 \to 4^+_1)$ is reasonably large for ^{132}Te and ^{134}Xe, and becomes sizably smaller for ^{136}Ba and ^{138}Ce, as given in Table III.

We now discuss the g factors of the 4^+_1 and the 6^+_1 states by using the method given by Lawson [62], according to which

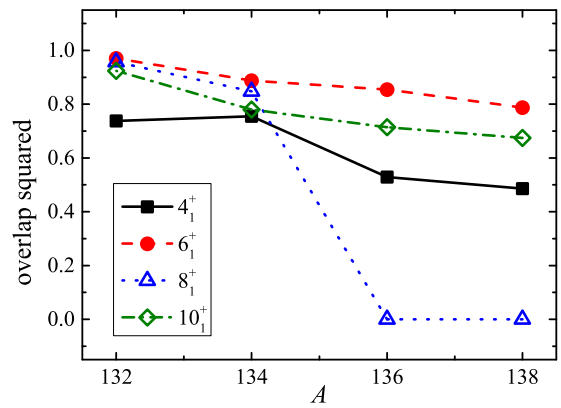

FIG. 5. The overlap squared between the proton (neutron) excitation configuration and the NPA wave function, versus mass number A. The solid squares and circles correspond to proton excitation, and the open triangles and diamonds correspond to neutron excitation. The black squares, red circles, blue triangles and green diamonds correspond to $|S^+_\nu\rangle \otimes |J_\pi = 4\rangle$ for the 4^+_1 states, $|S^+_\nu\rangle \otimes |J_\pi = 6\rangle$ for the 6^+_1 states, $|\mathcal{A}^{(8)}_\nu\rangle \otimes |(S^+_\pi)^{N_\pi/2}\rangle$ for the 8^+_1 states and $|\mathcal{A}^{(10)}_\nu\rangle \otimes |(S^+_\pi)^{N_\pi/2}\rangle$ for the 10^+_1 states, respectively.

the g factor of a state with configuration

$$\left[(\pi j)^{N_\pi}_{J_\pi} \times (\nu j')^{N_\nu}_{J_\nu}\right]_{JM} \tag{29}$$

can be written as

$$g = \tfrac{1}{2}[g_\pi(j) + g_\nu(j')] + \tfrac{1}{2}[g_\pi(j) - g_\nu(j')]X^J_{J_\pi J_\nu}.$$

Here $X^J_{J_\pi J_\nu} = \frac{J_\pi(J_\pi+1)-J_\nu(J_\nu+1)}{J(J+1)}$, and valence protons and neutrons occupy the j and j' orbits, respectively. N_σ and J_σ ($\sigma = \pi, \nu$) are particle numbers and spins. J is the total angular momentum and M is the z component of J. g_π (or g_ν) is the g factor for a single proton (or neutron) in the j (or j') orbit. For a system with proton excitation, $J_\nu = 0$, $J = J_\pi$, $X^J_{J_\pi J_\nu} = 1$; for a system with neutron excitation, $J_\pi = 0$, $J = J_\nu$, $X^J_{J_\pi J_\nu} = -1$. For protons in the $g_{7/2}$ orbit and neutrons in the $h_{11/2}$ orbit, $g_\pi(g_{7/2}) = 0.857\,\mu_N$ and $g_\nu(h_{11/2}) = -0.232\,\mu_N$ (taken from g factors of the lowest states with spin j in ^{133}Sb and ^{131}Sn, respectively). From these results, we have

$$g = \sum_{J_\pi J_\nu} A^2(J_\pi, J_\nu)(0.313 \pm 0.545)$$
$$= \begin{cases} 0.857\,\mu_N & \text{for proton excitation} \\ -0.232\,\mu_N & \text{for neutron excitation.} \end{cases} \tag{30}$$

$A(J_\pi, J_\nu)$ is the amplitude of the configuration. Because the 4^+_1 and the 6^+_1 states of ^{132}Te and ^{134}Xe are dominated by the proton excitation, $g = 0.857\,\mu_N$ for both the 4^+_1 and 6^+_1 states of ^{132}Te and ^{134}Xe. This value is quite close to the experimental data (0.79 and 0.80 μ_N) in Table IV.

D. 8^+_1 and 10^+_1 states

In Ref. [61], the 8^+_1 and 10^+_1 states of ^{132}Te were suggested to be of neutron excitations. Numerical calculations in Ref. [59] suggested that $|8^+_1\rangle = 0.96|\mathcal{A}^{(8)}_\nu \otimes S^+_\pi\rangle$ and $|10^+_1\rangle = 0.95|\mathcal{A}^{(10)}_\nu \otimes S^+_\pi\rangle - 0.24|\mathcal{A}^{(10)}_\nu \otimes D^+_\pi\rangle$. In the 50–82 major shell, if one constructs a nucleon pair with spin 8 or 10 and parity positive, the two valence nucleons (holes) must occupy the $h^-_{11/2}$ orbit. According to Table I, the single-particle energy of the $h^-_{11/2}$ orbit for protons (2.760 MeV) is much higher than that of neutrons (0.242 MeV). It is expected that the dominant components of the 8^+_1 and 10^+_1 states in ^{132}Te are of neutron excitations. Our calculated wave functions of these two states for ^{132}Te are

$$\begin{aligned} \left|8^+_1\right\rangle &= -0.98\left|\mathcal{A}^{(8)}_\nu \otimes S^+_\pi\right\rangle - 0.10\left|\mathcal{A}^{(8)}_\nu \otimes D^+_\pi\right\rangle \\ &\quad - 0.15\left|\mathcal{A}^{(6)}_\nu \otimes D^+_\pi\right\rangle + \cdots, \\ \left|10^+_1\right\rangle &= -0.96\left|\mathcal{A}^{(10)}_\nu \otimes S^+_\pi\right\rangle - 0.25\left|\mathcal{A}^{(10)}_\nu \otimes D^+_\pi\right\rangle \\ &\quad - 0.10\left|\mathcal{A}^{(8)}_\nu \otimes D^+_\pi\right\rangle + \cdots, \end{aligned} \tag{31}$$

respectively, which are very close to the results of Ref. [59]. On the other hand, weak mixings of proton D^+ pairs lead to an enhancement of $B(E2; 10^+_1 \to 8^+_1)$ values from ^{130}Sn to ^{132}Te, as observed experimentally [26]. Our calculated $B(E2; 10^+_1 \to 8^+_1)$ values reproduced this tendency very well, as shown in Table III.

In Fig. 5, we plot the overlap squared of the neutron excitation components, namely, $|\mathcal{A}^{(8)}_\nu\rangle \otimes |(S^+_\pi)^{N_\pi/2}\rangle$ for the 8^+_1 states and $|\mathcal{A}^{(10)}_\nu\rangle \otimes |(S^+_\pi)^{N_\pi/2}\rangle$ for the 10^+_1 states, with the NPA wave functions, versus the mass number A, denoted by blue triangles and green diamonds, respectively. According to Fig. 5, dominant components of the 10^+_1 states are the neutron excitation for all these four nuclei. However, the 8^+_1 states are dominated by the neutron excitation only for ^{132}Te and ^{134}Xe, and for ^{136}Ba and ^{138}Ce proton excitations becomes dominant. This change is represented in Table III, where our calculated $B(E2; 10^+_1 \to 8^+_1)$ values have a sudden decrease from ^{134}Xe to ^{136}Ba. This sudden change is given by the rapid decrease of neutron excitation components in the 8^+_1 state of the ^{136}Ba nucleus, as shown in Fig. 5. Because the 10^+_1 state of ^{138}Ce is dominated by the neutron excitation, according to Eq. (30),

$$g = -0.232\,\mu_N.$$

This is close to the corresponding experimental data ($-0.176\,\mu_N$), as listed in Table IV. Our calculated g factors of the 10^+_1 state for the other nuclei in Table IV are also close to this value. On the other hand, our calculated g factors of the 8^+_1 states in Table IV for ^{136}Ba and ^{138}Ce (≈0.64-0.69) are far from this value; this is consistent with the feature of their wave functions, which are not of neutron excitations, as pointed out above.

E. Negative parity states

We first look at negative parity states of ^{132}Te, plotted in Fig. 2(a). For this nucleus, the 5^-_1 and 7^-_1 states have been suggested to have two-neutron excitations [59–61,63,64], i.e., $|1h_{11/2}2d_{3/2}, J_\nu\rangle$ ($J = J_\nu = 5$ and 7). This is consistent with the experimentally observed tiny $B(E1, 7^-_1 \to 6^+_1) \approx 10^{-9}$ W.u. [65], if the 6^+_1 state is dominant of the proton excitation. According to Ref. [59], $|5^-_1\rangle = 0.97|H^-_\nu \otimes S^+_\pi\rangle$ and $|7^-_1\rangle = 0.96|\mathcal{J}^-_\nu \otimes S^+_\pi\rangle - 0.22|\mathcal{J}^-_\nu \otimes D^+_\pi\rangle$. In Ref. [61], the 7^-–13^- states are suggested to be nucleon-pair basis states of $|\mathcal{J}^-_\nu \otimes J_\pi\rangle$ with $J_\pi = 0$ - 6, where J_π is one proton pair with spin J_π; for the 9^-_1 state the proton pair is mainly D^+ and G^+, and for the 11^-_1 state the proton pair is mainly G^+ and I^+. According to our calculation, the wave functions of the lowest negative parity states are

$$\begin{aligned} |1^-_1\rangle &= 0.94|G^-_\nu \otimes G^+_\pi\rangle + \cdots, & |2^-_1\rangle &= -0.98|G^-_\nu \otimes D^+_\pi\rangle + \cdots, \\ |3^-_1\rangle &= -0.98|G^-_\nu \otimes D^+_\pi\rangle + \cdots, & |4^-_1\rangle &= -0.95|G^-_\nu \otimes S^+_\pi\rangle + \cdots, \\ |5^-_1\rangle &= -0.96|H^-_\nu \otimes S^+_\pi\rangle + \cdots, & |6^-_1\rangle &= -0.97|I^-_\nu \otimes S^+_\pi\rangle + \cdots, \\ |7^-_1\rangle &= -0.96|\mathcal{J}^-_\nu \otimes S^+_\pi\rangle + \cdots, & |8^-_1\rangle &= -0.97|\mathcal{J}^-_\nu \otimes D^+_\pi\rangle + \cdots, \\ |9^-_1\rangle &= 0.98|\mathcal{J}^-_\nu \otimes D^+_\pi\rangle + \cdots, & |10^-_1\rangle &= 0.86|\mathcal{J}^-_\nu \otimes J_\pi = 6\rangle + \cdots, \\ |11^-_1\rangle &= 0.83|\mathcal{J}^-_\nu \otimes J_\pi = 6\rangle + \cdots. \end{aligned} \tag{32}$$

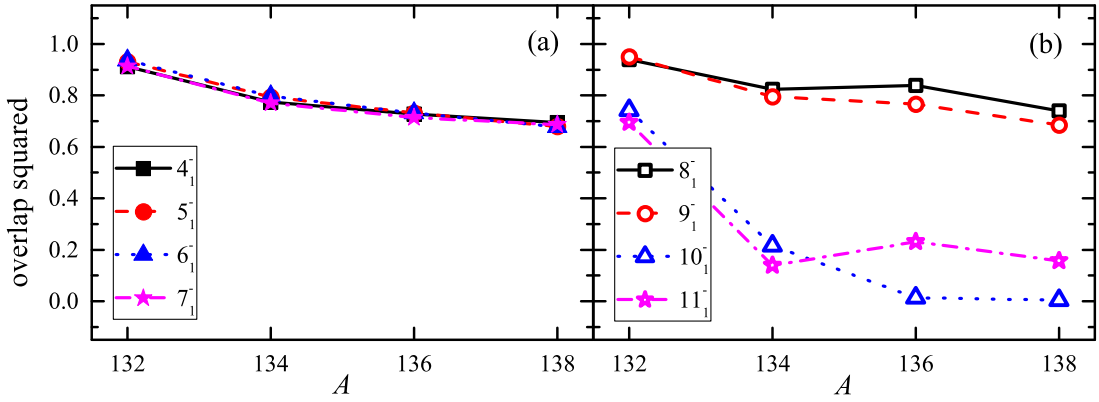

FIG. 6. The overlap squared between simple configurations of some J_1^- states in Eq. (32) and the NPA wave function, versus the mass number A. (a): $|J_\nu^- \otimes (S_\pi^+)^{N_\pi/2}\rangle$ (J_ν^- denotes G_ν^-, H_ν^-, I_ν^-, and $\mathcal{J}_\nu^-$ for 4_1^-, 5_1^-, 6_1^-, and 7_1^- states, respectively). (b): $|\mathcal{J}_\nu^-\rangle \otimes |J_\pi = 2\rangle$ configuration for the 8_1^-, 9_1^- states, and $|\mathcal{J}_\nu^-\rangle \otimes |J_\pi = 6\rangle$ configuration for the 10_1^-, 11_1^- states.

The energy levels of the 5_1^-, 6_1^-, and 7_1^- states are close to degenerate, and our calculated results have well reproduced these levels, as shown in Fig. 2(a). According to the above NPA wave functions, the $4_1^- - 7_1^-$ states are dominated by the neutron excitation, with weak mixings of proton D^+ pairs. Thus, these four states are the lowest negative parity states of ^{132}Te. The dominant components of the $8_1^- - 11_1^-$ states are $|\mathcal{J}_\nu^- \otimes D_\pi^+\rangle$ for $8_1^- - 9_1^-$ and $|\mathcal{J}_\nu^- \otimes I_\pi^+\rangle$ for $10_1^- - 11_1^-$, with small mixings of proton G^+ pairs. This is consistent with the results given in Ref. [61]. For the $1_1^- - 3_1^-$ states, the dominant components are G^- pair for the neutron part, and G^+ (for 1_1^+), D^+ pairs (for 2_1^+ and 3_1^+) for the proton part.

In Fig. 6, we plot the overlap squared versus the mass number A of a few negative-parity states for these nuclei. Figure 6(a) is the overlap squared between the neutron excitation configuration of the $4_1^- - 7_1^-$ states, i.e., $|J_\nu^- \otimes (S_\pi^+)^{N_\pi/2}\rangle$ (J_ν^- represents G^-, H^-, I^-, and $\mathcal{J}^-$ pair of neutron holes, respectively, for 4_1^-, 5_1^-, 6_1^-, and 7_1^- states) and corresponding NPA wave function of these four nuclei. It is shown that the $4_1^- - 7_1^-$ states of these four nuclei are all dominated by the neutron excitation. In Fig. 6(b), we plot the overlap squared between $|\mathcal{J}_\nu^- \otimes J_\pi = 2\rangle$ (the total spin of protons is two) configuration and the NPA wave function for the 8_1^-, 9_1^- states, and those between $|\mathcal{J}_\nu^- \otimes J_\pi = 6\rangle$ (the total spin of protons is six) configuration and the NPA wavefunction for the 10_1^-, 11_1^- states, respectively. The hollow black squares, red circles, blue triangles, and pink stars correspond to the 8_1^-, 9_1^-, 10_1^-, and 11_1^- states, respectively. One sees that the 8_1^- and 9_1^- states are all dominated by $|\mathcal{J}_\nu^- \otimes J_\pi = 2\rangle$ configuration for these nuclei. On the other hand, $|\mathcal{J}_\nu^- \otimes J_\pi = 6\rangle$ configuration in the 10_1^- and 11_1^- states is dominant only for the ^{132}Te nucleus.

F. Robustness of our calculated wave functions

In the above sections, we have constructed very simple nucleon-pair wave functions for yrast states, it is then very interesting and necessary to investigate the sensitivity of these results to the parameters optimized in Table II of this paper, in particular, the relative energies of valence proton pairs and valence neutron-hole pairs are apparently decisive to the dominant configurations of these states. Towards that goal, we have examined the robustness of these wave functions with respect to the modifications of the present parameters. Here, in order to save the computing time, for ^{136}Ba and ^{138}Ce we have not considered the contribution from the I'^+ (the second lowest spin-6) pair of proton, as it has been known that the I'^+ pair would not play any essential roles in the yrast states.

Our study of the above robustness is performed by two numerical experiments. The first experiment is done by adjusting one of two-body interaction parameters with other parameters fixed. Here, $\kappa_\pi^{(2)}(0)$, $\kappa_\nu^{(2)}(0)$, $G_\pi^{(2)}(0)$, and $G_\nu^{(2)}(0)$ are used to label the parameters employed in Secs. III A–E, whose values are given in Table II. The ranges of our parameters are as follows. $\kappa_\pi^{(2)}(0) - 0.005 \leqslant \kappa_\pi^{(2)} \leqslant \kappa_\pi^{(2)}(0) + 0.005$, $\kappa_\nu^{(2)}(0) - 0.005 \leqslant \kappa_\nu^{(2)} \leqslant \kappa_\nu^{(2)}(0) + 0.005$, $G_\pi^{(2)}(0) - 0.002 \leqslant G_\pi^{(2)} \leqslant G_\pi^{(2)}(0) + 0.002$, and $G_\nu^{(2)}(0) - 0.002 \leqslant G_\nu^{(2)} \leqslant G_\nu^{(2)}(0) + 0.002$. The parameters of monopole pairing interaction and proton-neutron quadrupole-quadrupole interaction have been long well refined and we do not make modifications in our numerical experiments. This numerical experiment shows that the only possible exception is the 8_1^+ states of ^{136}Ba and ^{138}Ce, which are dominated by the neutron excitation, but this artificial exception would not arise in reality, as it would contradict with the very small value of $B(E2, 10_1^+ \to 8_1^+)$: the 10_1^+ states of ^{136}Ba and ^{138}Ce are mainly given by the neutron excitation, and if the 8_1^+ states were the neutron excitation, the value of $B(E2, 10_1^+ \to 8_1^+)$ would be large.

Our second numerical experiment is done by adopting the parameters $\kappa_\pi^{(2)}$, $\kappa_\nu^{(2)}$, $G_\pi^{(2)}$, and $G_\nu^{(2)}$ randomly with the same ranges as in the above first numerical experiment. We have performed several sets of random $\kappa_\pi^{(2)}$, $\kappa_\nu^{(2)}$, $G_\pi^{(2)}$, and $G_\nu^{(2)}$, and adopt the same values for monopole pairing and quadrupole-quadrupole force between valence protons and valence neutron holes, for ^{132}Te, ^{134}Xe, and ^{136}Ba, respectively. This numerical experiment yields almost essentially the same results as our conclusion discussed above. According to our calculations, larger range of parameters may yield large deviations between calculated results and experimental values.

IV. SUMMARY

In this paper, we study the low-lying states of five even-even $N = 80$ isotones including ^{130}Sn, ^{132}Te, ^{134}Xe, ^{136}Ba, and ^{138}Ce within the nucleon-pair approximation (NPA). The low-lying energy spectra with both positive and negative parities are calculated, and most of them agree with the experimental data very well. $\mathcal{P}_\nu^{(10)\dagger}\cdot\tilde{\mathcal{P}}_\nu^{(10)}$ pairing interaction is shown to be necessary in reproducing the yrast 10^+ state by the analysis of ^{130}Sn by using a phenomenological pairing plus quadrupole Hamiltonian.

The wave functions of yrast $2_1^+-10_1^+$ states and $1_1^--11_1^-$ states of these nuclei are analyzed in detail. Most of these states have a very simple configuration in nucleon-pair basis. The 2_1^+ states of ^{132}Te, ^{134}Xe, ^{136}Ba, and ^{138}Ce are dominated by one D^+ neutron pair and $J_\pi = 2$ proton excitation. The 4_1^+ and 6_1^+ states of ^{132}Te and ^{134}Xe are well reproduced, and all these states are dominated by the proton excitation, while the 8_1^+ and 10_1^+ states are dominated by S^+ pairs of protons and one $J^{\text{parity}} = 8^+$ and 10^+ neutron pair, i.e., seniority-two excitation. For the negative parity states, the $4_1^--7_1^-$ states of ^{132}Te, ^{134}Xe, ^{136}Ba, and ^{138}Ce are dominated by S^+ pairs of protons and one $J^{\text{parity}} = 4^--7^-$ neutron pair, and the dominant configuration of the $8_1^--9_1^-$ states is $|\mathcal{J}_\nu^-\otimes J_\pi = 2\rangle$. The robustness of our parameters of Hamiltonian is discussed with two numerical experiments.

We calculate $B(E2)$ transition rates and g factors of low-lying states, which have a good agreement with experimental data. The calculated g factors are discussed based on single-j shells and Lawson's method. Some of the unknown $B(E2)$ values and g factors for low-lying states of these nuclei are predicted based on the NPA wave functions obtained in this paper.

ACKNOWLEDGMENTS

We thank the National Natural Science Foundation of China (Grants No. 11905130, No. 11875188, No. 11975151, No. 11961141003, and No. 11675101), Shanghai Sailing Program (Grant No. 19YF1434200), Shanghai Key Laboratory (Grant No. 11DZ2260700) and Open Foundation of Shanghai Key Laboratory of Particle Physics and Cosmology (Grant No. 18DZ2271500-3) for financial support.

APPENDIX A: EXPRESSION OF $q(jj\lambda)$ IN THE CASE OF SINGLE-j SHELL

In this Appendix, we give the expression of $q(ab\lambda)$, which is defined in Eq. (7) in the special case.

For nucleons in a single-j shell,

$$q(jj\lambda) = -\frac{\hat{j}}{\hat{\lambda}}R(jj\lambda)Y(jj\lambda), \tag{A1}$$

where

$$R(jj\lambda) = \frac{(2l+\lambda+1)!!}{(2l+1)!!}2^{-\lambda/2},$$

$$Y(jj\lambda) = (-1)^{j-1/2}\frac{\hat{j}\hat{\lambda}}{\sqrt{4\pi}}\begin{pmatrix} j & \lambda & j \\ -1/2 & 0 & 1/2\end{pmatrix}.$$

Here "()" in the right-hand side of $Y(jj\lambda)$ denotes the $3j$ symbol.

In the case of $\lambda = 2$, Eq. (A1) can be written as

$$\begin{aligned} q(jj2) &= -\frac{\hat{j}}{\hat{2}}R(jj2)Y(jj2) \\ &= -\frac{\hat{j}}{\hat{2}}\frac{2l+3}{2}(-1)^{j-1/2}\frac{\hat{j}\hat{2}}{\sqrt{4\pi}}\begin{pmatrix} j & 2 & j \\ -1/2 & 0 & 1/2\end{pmatrix} \\ &= (-1)^{j+1/2}\frac{(2j+1)(2l+3)}{4\sqrt{\pi}}\begin{pmatrix} j & 2 & j \\ -1/2 & 0 & 1/2\end{pmatrix}. \end{aligned}$$

For the $g_{7/2}$ orbit, $j = \frac{7}{2}$ and $l = 4$, thus

$$\begin{aligned} q\left(\frac{7}{2}\frac{7}{2}2\right) &= \frac{22}{\sqrt{\pi}}\begin{pmatrix} 7/2 & 2 & 7/2 \\ -1/2 & 0 & 1/2\end{pmatrix} \\ &= \frac{11}{2}\sqrt{\frac{10}{21\pi}}. \end{aligned} \tag{A2}$$

For the $h_{11/2}$ orbit, $j = \frac{11}{2}$ and $l = 5$, thus

$$\begin{aligned} q\left(\frac{11}{2}\frac{11}{2}2\right) &= \frac{39}{\sqrt{\pi}}\begin{pmatrix} 11/2 & 2 & 11/2 \\ -1/2 & 0 & 1/2\end{pmatrix} \\ &= \frac{13}{2}\sqrt{\frac{105}{143\pi}}. \end{aligned} \tag{A3}$$

In the case of $\lambda = 4$, Eq. (A1) can be written as

$$\begin{aligned} q(jj4) &= -\frac{\hat{j}}{\hat{4}}R(jj4)Y(jj4) \\ &= -\frac{\hat{j}}{\hat{4}}\frac{(2l+5)(2l+3)}{4}(-1)^{j-1/2}\frac{\hat{j}\hat{4}}{\sqrt{4\pi}} \\ &\quad\times\begin{pmatrix} j & 4 & j \\ -1/2 & 0 & 1/2\end{pmatrix} \\ &= (-1)^{j+1/2}\frac{(2j+1)(2l+5)(2l+3)}{8\sqrt{\pi}} \\ &\quad\times\begin{pmatrix} j & 4 & j \\ -1/2 & 0 & 1/2\end{pmatrix}. \end{aligned}$$

For the $h_{11/2}$ orbit, $j = \frac{11}{2}$ and $l = 5$, thus

$$\begin{aligned} q\left(\frac{11}{2}\frac{11}{2}4\right) &= \frac{585}{2\sqrt{\pi}}\begin{pmatrix} 11/2 & 4 & 11/2 \\ -1/2 & 0 & 1/2\end{pmatrix} \\ &= -195\sqrt{\frac{7}{286\pi}}. \end{aligned} \tag{A4}$$

Equations (A2), (A3), and (A4) are used in Sec. III and Appendix B.

APPENDIX B: OVERLAPS AND MATRIX ELEMENTS OF THE HAMILTONIAN FOR ONE AND TWO PAIRS

In this Appendix, we give expressions of the overlaps and matrix elements of $P^{(s)\dagger}\cdot P^{(s)}$ and $Q^{(t)}\cdot Q^{(t)}$ for one and two pairs, based on Ref. [24].

1. Overlaps

The expressions of the overlap for one and two pairs derived from Eq. (3.1) in Ref. [24] are the same as those given in Ref. [23]. According to Eq. (A.1) in Ref. [23], the overlap for one pair is

$$\langle s_1; J_1' | r_1; J_1 \rangle = 2\delta_{s_1,r_1} \sum_{ab} y(abr_1) y(abs_1). \tag{B1}$$

For nucleons in a single-j shell, Eq. (B1) can be further simplified to

$$\langle s_1; J_1' | r_1; J_1 \rangle = 2\delta_{s_1,r_1} y(jjr_1) y(jjs_1). \tag{B2}$$

According to Eq. (A.2) in Ref. [23], the overlap for two pairs is

$$\begin{aligned}\langle s_1 s_2; J_1' J_2' | r_1 r_2; J_1 J_2 \rangle &= 4\delta_{s_1,r_1}\delta_{s_2,r_2}\left[1 + (-1)^{r_1+r_2+J_2} \boldsymbol{p}_{r_1,r_2}\right] \sum_{aba'b'} y(a'b'r_1) y(a'b's_1) y(abr_2) y(abs_2) \\ &\quad - 16\hat{r}_1\hat{r}_2\hat{s}_1\hat{s}_2 \sum_{aa'bb'} y(a'as_1) y(b'bs_2) y(a'b'r_1) y(abr_2) \begin{Bmatrix} a' & a & s_1 \\ b' & b & s_2 \\ r_1 & r_2 & J_2 \end{Bmatrix},\end{aligned} \tag{B3}$$

where $\boldsymbol{p}_{r_1,r_2}$ is a permutation operator, which represents the exchange between r_1 and r_2, and "{ }" denotes the $9j$ symbol. For nucleons in a single-j shell, Eq. (B3) can be further simplified to

$$\begin{aligned}\langle s_1 s_2; J_1' J_2' | r_1 r_2; J_1 J_2 \rangle &= 4\delta_{s_1,r_1}\delta_{s_2,r_2}\left[1 + (-1)^{r_1+r_2+J_2} \boldsymbol{p}_{r_1,r_2}\right] y(jjr_1) y(jjs_1) y(jjr_2) y(jjs_2) \\ &\quad - 16\hat{r}_1\hat{r}_2\hat{s}_1\hat{s}_2 y(jjs_1) y(jjs_2) y(jjr_1) y(jjr_2) \begin{Bmatrix} j & j & s_1 \\ j & j & s_2 \\ r_1 & r_2 & J_2 \end{Bmatrix}.\end{aligned} \tag{B4}$$

2. Matrix elements of $P^{(s)\dagger} \cdot P^{(s)}$

According to Eq. (5.8) in Ref. [24], the matrix elements of $P^{(s)\dagger} \cdot P^{(s)}$ for an even system with $2n$ nucleons are

$$\begin{aligned}&\langle s_1 \cdots s_n; J_1' \cdots J_n' | P^{(s)\dagger} \cdot P^{(s)} | r_1 \cdots r_n; J_1 \cdots J_n \rangle \\ &= \delta_{J_n,J_n'} \sum_{k=n}^{1} \Bigg[\hat{s}\varphi_0 \delta_{r_k,s} \langle s_1 \cdots s_n; J_1' \cdots J_n' | r_1 \cdots r_{k-1} s r_{k+1} \cdots r_n; J_1 \cdots J_n \rangle \\ &\quad - \sum_{i=k-1}^{1} \sum_{t r_i' L_i \cdots L_{k-1}} (-1)^{t-s-r_k} \frac{\hat{t}}{\hat{r}_k} U(J_{k-1} t J_k s; L_{k-1} r_k) Q_{k-1}(t) \cdots Q_{i+1}(t) \bar{M}_i(t r_i') \\ &\quad \times \langle s_1 \cdots s_n; J_1' \cdots J_n' | r_1 \cdots \boldsymbol{r}_i' \cdots r_{k-1} s r_{k+1} \cdots r_n; J_1 \cdots J_{i-1} L_i \cdots L_{k-1} J_k \cdots J_n \rangle \Bigg],\end{aligned} \tag{B5}$$

where

$$\bar{M}_i(t r_i') = U(r_i t J_{i-1} L_i; r_i' J_i), \tag{B6}$$

$$Q_i(t) = (-1)^{J_{i-1}+L_i-J_i-L_{i-1}} U(r_i L_i J_{i-1} t; L_{i-1} J_i), \tag{B7}$$

with the convention

$$Q_n(t) \cdots Q_{k+1}(t) = \begin{cases} 1, & \text{for } k = n, \\ Q_n(t), & \text{for } k = n-1. \end{cases}$$

Here $U(abdc; ef) = \hat{e}\hat{f} W(abdc; ef)$, where $W(abdc; ef)$ is Racha coefficient. φ_0 in Eq. (B5) is defined as

$$\varphi_0 = \frac{2}{\hat{s}} \sum_{ab} y(abs) y_s(abs), \tag{B8}$$

where $y_s(abs)$ equals $\delta_{ab}\hat{j}_a/2$ or $q(abt)$ for $s = 0$ or t ($t = 2$ or 4). In the last line of Eq. (B5), $\boldsymbol{r}_i' \equiv \mathcal{B}^{r_i'\dagger}$ represents a new collective pair, i.e.,

$$\mathcal{B}^{r_i'\dagger} = \sum_{aa'} y'(aa'r_i') A^{r_i'\dagger}(aa'), \tag{B9}$$

where

$$y'(aa'r_i') = z(aa'r_i') - (-1)^{a+a'+r_i'} z(a'ar_i'), \tag{B10}$$

$$\begin{aligned}z(aa'r_i') &= 4\hat{r}_i\hat{r}_k\hat{s}\hat{t} \sum_{bb'} y_s(bb's) y(abr_k) y(a'b'r_i) \\ &\quad \times \begin{Bmatrix} r_k & s & t \\ b' & a & b \end{Bmatrix} \begin{Bmatrix} r_i & t & r_i' \\ a & a' & b' \end{Bmatrix}.\end{aligned} \tag{B11}$$

When $n = 1$, Eq. (B5) for one pair can be simplified to

$$\langle s_1; J_1' | P^{(s)\dagger} \cdot P^{(s)} | r_1; J_1 \rangle = \delta_{J_1,J_1'} \delta_{s_1,s} \hat{s} \varphi_0 \langle s_1; J_1' | s; J_1 \rangle.$$

Substituting Eqs. (B1) and (B8) into the above formula, and the matrix element

$$\langle s_1; J_1'|P^{(s)\dagger}\cdot P^{(s)}|r_1; J_1\rangle = 4\delta_{J_1,J_1'}\delta_{s_1,s}\left[\sum_{ab} y(abs_1)y_s(abs)\right]^2 \tag{B12}$$

can be obtained. For nucleons in a single-j shell, Eq. (B12) can be further simplified to

$$\langle s_1; J_1'|P^{(s)\dagger}\cdot P^{(s)}|r_1; J_1\rangle = 4\delta_{J_1,J_1'}\delta_{s_1,s}\big[y(jjs_1)y_s(jjs)\big]^2. \tag{B13}$$

When $n = 2$, Eq. (B5) for two pairs can be simplified to

$$\begin{aligned}\langle s_1s_2; J_1'J_2'|P^{(s)\dagger}\cdot P^{(s)}|r_1r_2; J_1J_2\rangle = \delta_{J_2,J_2'}\Bigg\{&\delta_{k,1}\hat{s}\varphi_0\delta_{r_1,s}\langle s_1s_2; J_1'J_2'|sr_2; J_1J_2\rangle + \delta_{k,2}\Bigg[\hat{s}\varphi_0\delta_{r_2,s}\langle s_1s_2; J_1'J_2'|r_1s; J_1J_2\rangle\\ &- \delta_{i,1}\sum_{tr_1'L_1}(-1)^{t-s-r_2}\frac{\hat{t}}{\hat{r}_2}U(J_1tJ_2s; L_1r_2)\bar{M}_1\big(tr_1'\big)\big\langle s_1s_2; J_1'J_2'\big|\boldsymbol{r}_1's; L_1J_2\big\rangle\Bigg]\Bigg\}.\end{aligned}$$

Substituting Eqs. (B6) and (B8) into the above formula, and the matrix element

$$\begin{aligned}\langle s_1s_2; J_1'J_2'|P^{(s)\dagger}\cdot P^{(s)}|r_1r_2; J_1J_2\rangle = \delta_{J_2,J_2'}\Bigg\{&2[1+(-1)^{r_1+r_2+J_2}\boldsymbol{p}_{r_1,r_2}]\delta_{r_2,s}\sum_{ab} y(abs)y_s(abs)\langle s_1s_2; J_1'J_2'|r_1s; J_1J_2\rangle\\ &- \sum_{tr_1'}(-1)^{t-s-r_2}\hat{t}\hat{r}_1'W(J_1tJ_2s; r_1'r_2)\langle s_1s_2; J_1'J_2'|\boldsymbol{r}_1's; r_1'J_2\rangle\Bigg\}\end{aligned} \tag{B14}$$

can be obtained. The overlaps for two pairs in the above formula are given by Eq. (B3), with $y(abr_2)$ replaced by $y_s(abs)$, and $y(a'b'r_1)$ in the second overlap replaced by $y'(a'b'r_1')$, which is defined in Eq. (B10). For nucleons in a single-j shell, Eq. (B14) can be further simplified to

$$\begin{aligned}\langle s_1s_2; J_1'J_2'|P^{(s)\dagger}\cdot P^{(s)}|r_1r_2; J_1J_2\rangle = \delta_{J_2,J_2'}\Bigg\{&2[1+(-1)^{r_1+r_2+J_2}\boldsymbol{p}_{r_1,r_2}]\delta_{r_2,s}y(jjr_2)y_s(jjs)\langle s_1s_2; J_1'J_2'|r_1s; J_1J_2\rangle\\ &- \sum_{tr_1'}(-1)^{t-s-r_2}\hat{t}\hat{r}_1'W(J_1tJ_2s; r_1'r_2)\langle s_1s_2; J_1'J_2'|\boldsymbol{r}_1's; r_1'J_2\rangle\Bigg\}.\end{aligned} \tag{B15}$$

Here the overlaps are given by Eq. (B4), with $y(jjr_2)$ replaced by $y_s(jjs)$, and $y(jjr_1)$ in the second overlap replaced by $y'(jjr_1')$, where

$$y'(jjr_1') = [1+(-1)^{r_1'}]4\hat{r}_1\hat{r}_2\hat{s}\hat{t}y_s(jjs)y(jjr_2)y(jjr_1)\begin{Bmatrix} r_2 & s & t\\ j & j & j\end{Bmatrix}\begin{Bmatrix} r_1 & t & r_1'\\ j & j & j\end{Bmatrix}.$$

3. Matrix elements of $Q^{(t)}\cdot Q^{(t)}$

According to Eq. (5.5) in Ref. [24], the matrix elements of $Q^{(t)}\cdot Q^{(t)}$ for an even system with $2n$ nucleons is

$$\begin{aligned}&\langle s_1\cdots s_n; J_1'\cdots J_n'|Q^{(t)}\cdot Q^{(t)}|r_1\cdots r_n; J_1\cdots J_n\rangle\\ &= \sum_{k=n}^{1}\Bigg[\sum_{r_k'}(-1)^{r_k'-r_k-t}\frac{\hat{r}_k'}{\hat{r}_k}\langle s_1\cdots s_n; J_1'\cdots J_n'|r_1\cdots\boldsymbol{r}_kr_{k+1}\cdots r_n; J_1\cdots J_n\rangle\\ &\quad+\sum_{i=k-1}^{1}\sum_{r_i'r_k'L_i\cdots L_{k-1}}2\frac{\hat{r}_k'}{\hat{r}_k}U(J_{k-1}tJ_kr_k'; L_{k-1}r_k)Q_{k-1}(t)\cdots Q_{i+1}(t)\bar{M}_i(tr_i')\\ &\quad\times\langle s_1\cdots s_n; J_1'\cdots J_n'|r_1\cdots\boldsymbol{r}_i'\cdots\boldsymbol{r}_k'\cdots r_n; J_1\cdots J_{i-1}L_i\cdots L_{k-1}J_k\cdots J_n\rangle\Bigg].\end{aligned} \tag{B16}$$

Here $\boldsymbol{r}_k \equiv \tilde{\boldsymbol{B}}^{r_k}(r'_k)$, which is defined as

$$\begin{aligned}\tilde{\boldsymbol{B}}^{r_k}(r'_k) &= [\tilde{A}^{r'_k}, Q^{(t)}]^{(r_k)} = [[\tilde{A}^{r_k}, Q^{(t)}]^{(r'_k)}, Q^{(t)}] \\ &= \sum_{ab} \bar{y}(abr_k)\tilde{A}^{r_k}(ab),\end{aligned} \tag{B17}$$

with

$$\bar{y}(abr_k) = \bar{z}(abr_k) - (-1)^{a+b+r_k}\bar{z}(bar_k), \tag{B18}$$

$$\bar{z}(abr_k) = 2\hat{r}'_k\hat{r}_k(2t+1)\sum_{dd'} y(dd'r_k)q(d'bt)q(dat)\begin{Bmatrix} r_k & t & r'_k \\ b & d & d' \end{Bmatrix}\begin{Bmatrix} r_k & t & r'_k \\ d & b & a \end{Bmatrix}. \tag{B19}$$

In the last line of Eq. (B16), $\boldsymbol{r}'_i$ and $\boldsymbol{r}'_k$ are defined as

$$\tilde{\mathcal{A}}^{r'_k} = [\tilde{A}^{r_k}, Q^{(t)}]^{(r'_k)} = \sum_{ad} y'(dar'_k)\tilde{A}^{r'_k}(da),$$

where

$$y'(dar'_k) = z(dar'_k) - (-1)^{d+a+r'_k}z(adr'_k), \tag{B20}$$

$$z(dar'_k) = \hat{r}_k\hat{t}\sum_b y(abr_k)q(bdt)\begin{Bmatrix} r_k & t & r'_k \\ d & a & b \end{Bmatrix}. \tag{B21}$$

When $n = 1$, Eq. (B16) for one pair can be simplified to

$$\begin{aligned}\langle s_1; J'_1|Q^{(t)}\cdot Q^{(t)}|r_1; J_1\rangle &= \sum_{r'_1}(-1)^{r'_1-r_1-t}\frac{\hat{r'_1}}{\hat{r}_1}\langle s_1; J'_1|\boldsymbol{r}_1; J_1\rangle \\ &= 2\delta_{s_1,r_1}\sum_{r'_1}(-1)^{r'_1-r_1-t}\frac{\hat{r'_1}}{\hat{r}_1}\sum_{ab}\bar{y}(abr_1)y(abs_1),\end{aligned} \tag{B22}$$

where $\bar{y}(abr_1)$ is given by Eq. (B18). For nucleons in a single-j shell with $t = 2$, Eq. (B22) can be further simplified to

$$\langle s_1; J'_1|Q^{(2)}\cdot Q^{(2)}|r_1; J_1\rangle = 2\delta_{s_1,r_1}\sum_{r'_1}(-1)^{r'_1-r_1-t}\frac{\hat{r'_1}}{\hat{r}_1}\bar{y}(jjr_1)y(jjs_1), \tag{B23}$$

with

$$\bar{y}(jjr_1) = 20\hat{r}'_1\hat{r}_1 y(jjr_1)[q(jj2)]^2\begin{Bmatrix} r_1 & 2 & r'_1 \\ j & j & j \end{Bmatrix}^2. \tag{B24}$$

For $j = 7/2$ or $11/2$, the value of $q(jj2)$ is given in Eq. (A2) or Eq. (A3).

When $n = 2$, Eq. (B16) for two pairs can be simplified to

$$\begin{aligned}\langle s_1s_2; J'_1J'_2|Q^{(t)}\cdot Q^{(t)}|r_1r_2; J_1J_2\rangle &= \delta_{k,1}\sum_{r'_1}(-1)^{r'_1-r_1-t}\frac{\hat{r'_1}}{\hat{r}_1}\langle s_1s_2; J'_1J'_2|\boldsymbol{r}_1r_2; J_1J_2\rangle + \delta_{k,2}\Bigg[\sum_{r'_2}(-1)^{r'_2-r_2-t}\frac{\hat{r'_2}}{\hat{r}_2}\langle s_1s_2; J'_1J'_2|r_1\boldsymbol{r}_2; J_1J_2\rangle \\ &\quad + \delta_{i,1}\sum_{r'_1r'_2L_1} 2\frac{\hat{r'_2}}{\hat{r}_2}U(J_1tJ_2r'_2; L_1r_2)\bar{M}_1(tr'_1)\langle s_1s_2; J'_1J'_2|\boldsymbol{r}'_1\boldsymbol{r}'_2; L_1J_2\rangle\Bigg].\end{aligned}$$

Substituting Eq. (B6) into the above formula, and the matrix element

$$\begin{aligned}\langle s_1s_2; J'_1J'_2|Q^{(t)}\cdot Q^{(t)}|r_1r_2; J_1J_2\rangle &= \left[1 + (-1)^{r_1+r_2+J_2}\boldsymbol{p}_{r_1,r_2}\right]\sum_{r'_1}(-1)^{r'_1-r_1-t}\frac{\hat{r'_1}}{\hat{r}_1}\langle s_1s_2; J'_1J'_2|\boldsymbol{r}_1r_2; J_1J_2\rangle \\ &\quad + \sum_{r'_1r'_2} 2\hat{r'_1}\hat{r'_2}W(J_1tJ_2r'_2; r'_1r_2)\langle s_1s_2; J'_1J'_2|\boldsymbol{r}'_1\boldsymbol{r}'_2; r'_1J_2\rangle\end{aligned} \tag{B25}$$

can be obtained. Here overlaps for two pairs in the above formula are given by Eq. (B3), with $y(a'b'r_1)$ in the first overlap replaced by $\bar{y}(a'b'r_1)$, which is defined in Eq. (B18), and $y(a'b'r_1)$ and $y(abr_2)$ in the second overlap replaced by $y'(a'b'r_1')$ and $y'(abr_2')$, which are defined in Eq. (B20), respectively. For nucleons in a single-j shell with $t = 2$, the overlaps are given by Eq. (B4), with $y(jjr_1)$ in the first overlap replaced by $\bar{y}(jjr_1)$, i.e., Eq. (B24), and $y(jjr_k)$ ($k = 1$ and 2) in the second overlap replaced by $y'(jjr_k')$, where

$$y'(jjr_k') = 2\sqrt{5}\hat{r}_k y(jjr_k) q(jj2) \begin{Bmatrix} r_k & 2 & r_k' \\ j & j & j \end{Bmatrix}.$$

For $j = 7/2$ or $11/2$, the value of $q(jj2)$ is in Eq. (A2) or Eq. (A3).

[1] M. G. Mayer, Phys. Rev. **74**, 235 (1948); **75**, 1969 (1949); **78**, 16 (1950).
[2] S. E. Koonin, D. J. Dean, and K. Langanke, Phys. Rep. **278**, 1 (1997).
[3] T. Otsuka, M. Honma, T. Mizusaki, N. Shimizu, and Y. Utsuno, Prog. Part. Nucl. Phys. **47**, 319 (2001).
[4] E. Caurier, G. Martinez-Pinedo, F. Nowack, A. Poves, and A. P. Zuker, Rev. Mod. Phys. **77**, 427 (2005).
[5] Y. M. Zhao, S. Yamaji, N. Yoshinaga, and A. Arima, Phys. Rev. C **62**, 014315 (2000); Y. M. Zhao, N. Yoshinaga, S. Yamaji, and A. Arima, *ibid.* **62**, 024322 (2000).
[6] L. Y. Jia, H. Zhang, and Y. M. Zhao, Phys. Rev. C **75**, 034307 (2007); **76**, 054305 (2007).
[7] L. H. Zhang, H. Jiang, and Y. M. Zhao, Sci. China Phys. Mech. Astron. **54**, 103 (2011).
[8] Y. Lei, Y. M. Zhao, and A. Arima, Phys. Rev. C **84**, 044301 (2011); Y. Lei and Z. Y. Xu, *ibid.* **92**, 014317 (2015).
[9] Y. Lei, G. J. Fu, and Y. M. Zhao, Phys. Rev. C **87**, 044331 (2013).
[10] H. Jiang, Y. Lei, G. J. Fu, Y. M. Zhao, and A. Arima, Phys. Rev. C **86**, 054304 (2012).
[11] H. Jiang, Y. Lei, C. Qi, R. Liotta, R. Wyss, and Y. M. Zhao, Phys. Rev. C **89**, 014320 (2014).
[12] Y. Y. Cheng, Y. Lei, Y. M. Zhao, and A. Arima, Phys. Rev. C **92**, 064320 (2015); Y. Y. Cheng, Y. M. Zhao, and A. Arima, *ibid.* **94**, 024307 (2016).
[13] X. W. Pan, J. L. Ping, D. H. Feng, J. Q. Chen, C. L. Wu, and M. W. Guidry, Phys. Rev. C **53**, 715 (1996).
[14] Y. A. Luo, J. Q. Chen, T. F. Feng, and P. Z. Ning, Phys. Rev. C **64**, 037303 (2001); Y. A. Luo, X. B. Zhang, F. Pan, P. Z. Ning, and J. P. Draayer, *ibid.* **64**, 047302 (2001).
[15] K. Higashiyama, N. Yoshinaga, and K. Tanabe, Phys. Rev. C **65**, 054317 (2002).
[16] K. Sieja, G. Martínez-Pinedo, L. Coquard, and N. Pietralla, Phys. Rev. C **80**, 054311 (2009).
[17] K. Higashiyama and N. Yoshinaga, Phys. Rev. C **83**, 034321 (2011).
[18] E. Teruya, N. Yoshinaga, K. Higashiyama, and A. Odahara, Phys. Rev. C **92**, 034320 (2015).
[19] K. Higashiyama, N. Yoshinaga, and K. Tanabe, Phys. Rev. C **67**, 044305 (2003).
[20] Y. M. Zhao, N. Yoshinaga, S. Yamaji, and A. Arima, Phys. Rev. C **62**, 014316 (2000).
[21] Z. Y. Xu, Y. Lei, Y. M. Zhao, S. W. Xu, Y. X. Xie, and A. Arima, Phys. Rev. C **79**, 054315 (2009).
[22] H. Jiang, C. Qi, Y. Lei, R. Liotta, R. Wyss, and Y. M. Zhao, Phys. Rev. C **88**, 044332 (2013).
[23] J. Q. Chen, Nucl. Phys. A **626**, 686 (1997).
[24] Y. M. Zhao, N. Yoshinaga, S. Yamaji, J. Q. Chen, and A. Arima, Phys. Rev. C **62**, 014304 (2000).
[25] B. Fogelberg, K. Heyde, and J. Sau, Nucl. Phys. A **352**, 157 (1981).
[26] J. Genevey, J. A. Pinston, C. Foin, M. Rejmund, R. F. Casten, H. Faust, and S. Oberstedt, Phys. Rev. C **63**, 054315 (2001).
[27] G. Lo Bianco, P. Paruzzi, K. P. Schmittgen, R. Reinhardt, A. Gelberg, K. O. Zell, P. von Brentano, and N. Blasi, Nucl. Phys. A **470**, 266 (1987).
[28] J. C. Merdinger, F. A. Beck, E. Bozek, T. Byrski, C. Gehringer, Y. Schutz, and J. P. Vivien, Nucl. Phys. A **346**, 281 (1980).
[29] M. Lach, J. Styczen, R. Julin, M. Piiparinen, H. Beuscher, P. Kleinheinz, and J. Blomqvist, Z. Phys. A **319**, 235 (1984).
[30] H. A. Roth, S. E. Arnell, D. Foltescu, Ö. Skeppstedt, J. Blomqvist, G. de Angelis, D. Bazzacco, and S. Lunardi, Eur. Phys. J. A **10**, 275 (2001).
[31] J. J. Valiente-Dobón *et al.*, Phys. Rev. C **69**, 024316 (2004).
[32] T. Shizuma, Z. G. Gan, K. Ogawa, H. Nakada, M. Oshima, Y. Toh, T. Hayakawa, Y. Hatsukawa, M. Sugawara, Y. Utsuno, and Z. Liu, Eur. Phys. J. A **20**, 207 (2004).
[33] Y. M. Zhao and A. Arima, Phys. Rep. **545**, 1 (2014).
[34] G. J. Fu, Y. Lei, Y. M. Zhao, S. Pittel, and A. Arima, Phys. Rev. C **87**, 044310 (2013).
[35] Y. Y. Cheng, Y. M. Zhao, and A. Arima, Phys. Rev. C **97**, 024303 (2018).
[36] C. Qi, J. Blomqvist, T. Bäck, B. Cederwall, A. Johnson, R. J. Liotta, and R. Wyss, Phys. Rev. C **84**, 021301(R) (2011).
[37] Z. X. Xu, C. Qi, J. Blomqvist, R. J. Liotta, and R. Wyss, Nucl. Phys. A **877**, 51 (2012).
[38] P. Van Isacker, A. O. Macchiavelli, P. Fallon, and S. Zerguine, Phys. Rev. C **94**, 024324 (2016).
[39] P. Van Isacker, J. Engel, and K. Nomura, Phys. Rev. C **96**, 064305 (2017).
[40] L. Y. Jia, Phys. Rev. C **93**, 064307 (2016); **96**, 034313 (2017).
[41] L. Y. Jia and C. Qi, Phys. Rev. C **94**, 044312 (2016).
[42] M. A. Caprio, F. Q. Luo, K. Cai, V. Hellemans, and Ch. Constantinou, Phys. Rev. C **85**, 034324 (2012).
[43] M. A. Caprio, F. Q. Luo, K. Cai, Ch. Constantinou, and V. Hellemans, J. Phys. G: Nucl. Part. Phys. **39**, 105108 (2012).
[44] B. Fogelberg and J. Blomqvist, Nucl. Phys. A **429**, 205 (1984).
[45] W. J. Baldridge, Phys. Rev. C **18**, 530 (1978).
[46] ENSDF Viewer, National Nuclear Data Center, http://ie.lbl.gov/ensdf/.
[47] Y. Lei, Z. Y. Xu, Y. M. Zhao, and A. Arima, Phys. Rev. C **80**, 064316 (2009).
[48] H. Kusakari, M. Sugawara, M. Fujioka, N. Kawamura, S. Hayashibe, K. Iura, F. Sakai, and T. Ishimatsu, Phys. Rev. C **30**, 820 (1984).
[49] P. Das, R. G. Pillay, V. V. Krishnamurthy, S. N. Mishra, and S. H. Devare, Phys. Rev. C **53**, 1009 (1996).
[50] D. C. Radford *et al.*, Nucl. Phys. A **746**, 83 (2004).

[51] G. Rainovski, N. Pietralla, T. Ahn, C. J. Lister, R. V. F. Janssens, M. P. Carpenter, S. Zhu, and C. J. Barton, Phys. Rev. Lett. **96**, 122501 (2006).
[52] N. J. Stone, At. Data Nucl. Data Tables **90**, 75 (2005).
[53] D. C. Radford *et al.*, Phys. Rev. Lett. **88**, 222501 (2002).
[54] M. Danchev *et al.*, Phys. Rev. C **84**, 061306(R) (2011).
[55] F. Iachello and A. Arima, *The Interacting Boson Model* (Cambridge University Press, Cambridge, 1987).
[56] T. Alharbi *et al.*, Phys. Rev. C **87**, 014323 (2013).
[57] A. Hussain, F. Al-Khudair, and A. Subber, Turk. J. Phys. **39**, 137 (2015).
[58] J. M. Allmond *et al.*, Phys. Rev. C **87**, 054325 (2013).
[59] J. Sau, K. Heyde, and R. Chery, Phys. Rev. C **21**, 405 (1980).
[60] R. O. Hughes *et al.*, Phys. Rev. C **69**, 051303(R) (2004).
[61] S. Biswas *et al.*, Phys. Rev. C **93**, 034324 (2016).
[62] R. D. Lawson, *Theory of the Nuclear Shell Model* (Clarendon Press, Oxford, 1980).
[63] A. Kerek, P. Carle, and S. Borg, Nucl. Phys. A **224**, 367 (1974).
[64] R. O. Hughes, N. V. Zamfir, D. C. Radford, C. J. Gross, C. J. Barton, C. Baktash, M. A. Caprio, R. F. Casten, A. Galindo-Uribarri, P. A. Hausladen, E. A. McCutchan, J. J. Ressler, D. Shapira, D. W. Stracener, and C.-H. Yu, Phys. Rev. C **71**, 044311 (2005).
[65] Yu. V. Sergeenkov, Nucl. Data Sheets **65**, 277 (1992).